Journal of the European Ceramic Society **9** (1992) 427–435

The Acoustic Emission Analysis of the Crack Processes in Alumina

C. Sklarczyk

Fraunhofer-Institut für zerstörungsfreie Prüfverfahren, Universität des Saarlandes, Gebäude 37, D-6600 Saarbrücken 11, FRG

(Received 20 August 1991; accepted 17 September 1991)

Abstract

The crack processes in single-phase alumina specimens have been investigated by acoustic emission (AE) analysis with regard to the increase of the crack resistance. During loading of a notched specimen, individual AE signals are observed at first, which are probably due to the generation of microcracks in a process zone around the notch. At higher loads signal clusters are found, which should be due to the coalescence of microcracks. By these coalescence events the main crack is formed. At macroscopic crack propagation most AE events are located within the crack tip zone. However, up to about 20% of all events are located within the crack flank zone behind the crack tip. Thus, it can be concluded that there is an energy dissipation at the crack tip at beginning of the loading, which determines the starting value of the crack resistance. At macroscopic crack propagation crack flank interactions contribute to the increase of crack resistance, too. However, it cannot be decided from AE if the contribution of the process zone at the crack tip or of the crack flanks in the wake of the crack tip play the major role in increasing the crack resistance.

Die Rißausbreitung in einphasigen Aluminiumoxidproben wurde mit der akustischen Emissionsanalyse (AE) auf die Zunahme des Rißwiderstandes hin untersucht. Bei der Belastung einer gekerbten Probe wurden zunächst einzelne AE-Signale beobachtet, die wahrscheinlich auf die Entstehung von Mikrorissen in der Prozeßzone um die Kerbe zurückzuführen sind. Bei höheren Belastungen treten Signalhäufungen auf, die auf das Zusammenwachsen von Mikrorissen hinweisen. Aus diesem Zusammenwachsen bildet sich der Hauptriß. Während der makroskopischen Rißausbreitung treten die meisten AE-Signale innerhalb der Rißspitzenzone auf. Jedoch können bis zu 20% aller Signale innerhalb der Rißflankenzone hinter der Rißspitze lokalisiert sein. Es kann somit gefolgert werden, daß es bei Belastungsbeginn an der Rißspitze zu einer Energiedissipation kommt, die den Ausgangswert des Rißwiderstandes bestimmt. Beim makroskopischen Rißwachstum tragen die Wechselwirkungen mit der Rißflanke ebenfalls zu einer Erhöhung des Rißwiderstandes bei. Es kann jedoch mit AE-Daten nicht geklärt werden, ob die Prozeßzone an der Rißspitze oder die Rißflankenzonen in der Spur der Rißspitze den Hauptteil an der Erhöhung des Rißwiderstandes tragen.

On a étudié les mécanismes de fissuration dans des échantillons d'alumine monophasés par émission acoustique (AE), notamment en ce qui concerne l'augmentation de la résistance à la fissuration. Pendant le chargement d'un échantillon entaillé, on observe d'abord des signaux acoustiques isolés, qui sont probablement dûs à la formation de microfissures dans une zone d'endommagement autour de l'entaille. A charge plus élevée, on trouve des groupes de signaux qui s'expliquent certainement par la coalescence des microfissures. La fissure principale est formée par ces phénomènes de coalescence. Lors de la propagation macroscopique de la fissure, la plupart des pulses acoustiques provient de l'extrémité de la fissure. Pourtant, jusqu'à 20% de l'ensemble des événements émanent d'une zone située dans la flanc de la fissure, derrière l'extrémité de la fissure. On en conclut qu'il y a dissipation d'énergie à l'extrémité de la fissure au début du chargement, ce qui détermine la résistance initiale à la fissuration. Puis pendant la propagation macroscopique de la fissure, des interactions provenant des zones discrètes adjacentes à la fissure contribuent également à l'augmentation de la résistance à la fissuration. Toutefois, on ne peut

Journal of the European Ceramic Society 0955-2219/92/$5.00

déterminer, à partir des mesures d'émission acoustique, quelle contribution—celle de la zone d'endommagement en avant du front de fissure ou celle de la zone située sur les flancs de la fissure dans le sillage de l'extrémité de la fissure, joue le rôle principal quant à l'augmentation de la résistance à la fissuration.

1 Introduction

1.1 Increase of crack resistance

During controlled crack propagation experiments on many ceramics, e.g. single-phase alumina, an increase of the crack resitance $R = dU/da$ (where U is the energy necessary for crack propagation and a is the crack depth) as crack depth grows is observed.[1] Since there is no plastic deformation at room temperature an explanation for this phenomenon is sought. The principal approaches are the process zone model and the crack surface interaction model.

According to the process zone model an array of microcracks ahead of the main crack is formed during crack propagation.[2] The microcracks are preferably generated at the grain boundaries. The microcrack array partially shields the tip of the main crack and thus diminishes the stress intensity factor K. Some additional decrease of K is due to residual stresses produced at the damaged crack borders.[3] The main crack proceeds in such a way that the microcracks coalesce.

According to the other model the increase of R is caused by the energy dissipating interaction of the rough serrated crack faces.[4,5] Linkage points by protruding grains are formed. To separate these points, an additional energy is required so that the R-value grows. This separation may be done by friction processes or by new cracks behind the crack tip which run around the protruding grain. The interaction length of the crack faces is the larger the grain size and lies in the most cases in the order of magnitude of a few mm.

1.2 Fundamentals of acoustic emission analysis

During the sudden release of stored energy in a material sound waves are produced. This phenomenon is called acoustic emission (AE). The frequency range of AE extends from low frequency to the MHz range. The formation of micro- and macrocracks as well as friction processes are sources of acoustic emission. The AE signals can be captured with sensors which are mostly of the piezoelectric type and are attached on the surface of the object under investigation. The amplified signals are then processed and stored by equipment normally based on a computer. To save mass storage and to increase the speed of data acquisition the complex AE–time signals are compressed by hard- or software to a few characteristic signals parameters like the peak amplitude, signal duration, energy or risetime (time between beginning and maximum of the signal). By using more than one sensor it is possible to locate the AE sources, e.g. by calculating the source position from the arrival time differences between the sensors. Thus, it should be possible by an accurate localization of AE sources to separate crack tip and crack flank related AE events and to get insight into the mechanism of R-curve rising. Additionally, the AE analysis can give some information on the first formation of the micro-crack array and on coalescence of microcracks.

2 Experimental Conditions

2.1 Specimens

The specimens were made from alumina type AF 997 from Desmarquest (Evreux, France) with an intergranular fracture mode, a mean grain size of about 10 μm and a purity of 99·5%. The used specimen geometries were as follows:

—DCB (double cantilever beam) specimens: length 50 mm, width 25 mm, thickness 0·8 or 1·3 mm, notch depth 7·5–9·5 mm, notch width 0·15–0·3 mm. A scheme with the loading points and the positioning of the transducers is shown in Fig. 1. The zone near to the crack tip of these specimens was checked before and after loading by a scanning electron microscope (SEM) and by small angle X-ray scattering (SAXS). The last method gives information on the increase of scattering centres in the specimen induced by loading.[6]

—SENB (single end notched bending) specimens for four-point bending tests from the same material: length 130 mm, width 5 mm, height 15 mm, notch depth 4·7–5 mm, notch width 50 μm (Fig. 2). The crack tip could be pursued by a travelling microscope with video equipment so that the crack depth was measured throughout the whole test with the help of a displacement measuring unit. The accuracy of crack depth measurement was 150–300 μm.

The tests on the DCB specimens were done with a small specially designed loading device. The experiments on the bending specimens were conducted with an hydraulic MTS machine and could be controlled by load and displacement.

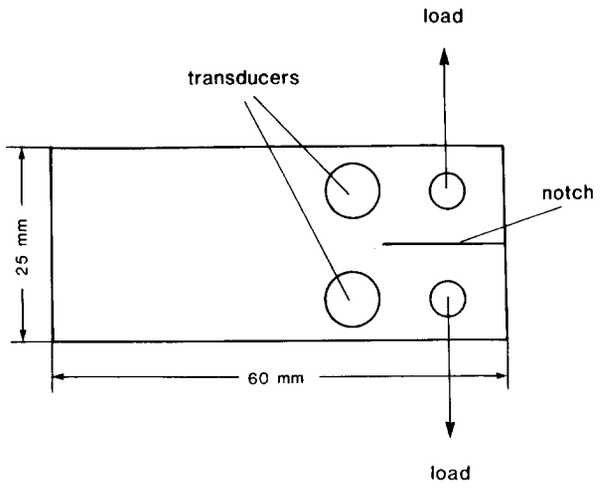

Fig. 1. Transducer positioning on a 0·8 mm thick DCB specimen of alumina.

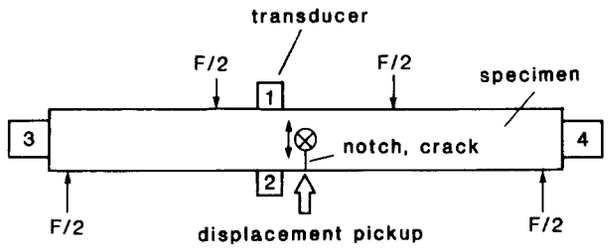

Fig. 2. Transducer arrangement on an alumina specimen. ⊗, Microscope lens; F, force.

2.2 AE equipment

To capture the AE piezoelectric transducers were attached to the specimens. For the DCB specimens high-sensitivity resonant Nano30 sensors (resonance frequency 300 kHz) from PAC (Princeton, NJ, USA) were used, whereas for the SENB specimens broadband V133 transducers (2·25 MHz) from Panametrics (Waltham, MA, USA) and resonant high-frequency transducers (7·5 MHz) from Minhorst (Meudt, FRG) (specially made for this investigation) were used. The sensors were fixed on to the specimens by a quickly hardened two-component glue from UHU (Bühl, FRG) or by a coupling wax from AET (Sacramento, CA, USA).

The transducers were arranged in such a way on the specimens that disturbance noise from the loading points could be separated from genuine AE by localization (Figs 1 and 2). The Minhorst sensors 1 and 2 in Fig. 2 were used for the accurate localization of AE sources in the crack plane. Localization accuracy was in the range of ± 1 mm. For these experiments, modified preamplifiers from Panametrics with a bandwidth of 26 kHz–15 MHz were applied in conjunction with high pass filters of 100 kHz to suppress parasitic noise from the loading device. These trials were carried out in cooperation with the Forschungszentrum Jülich (Jülich, FRG).

A six-channel digital AE equipment[7] was used which was designed, developed and built by IzfP (Saarbrücken, FRG). With the help of a real-time hardware signal processor it determines for each signal the parameters: risetime, peak amplitude, energy, duration and arrival time. The maximum signal processing speed is 40 000 signals/s (for minimum dead time) for short times and 1500 signals/s for long times. Storage and evaluation of the data is performed by a μVax/GPX-Workstation from DEC (Nashua, NH, USA) in conjunction with a mass storage with a capacity of several million signals. Additionally an array-processor from CSPI (Billerica, MA, USA) is integrated in the AE system which allows the acquisition and storage of a limited number of time signals (maximum 8000) with a maximum sample rate of 10 MHz. These time signals can be regarded as a representative sample of the totality of AE signals and help to interpret the frequency distributions of the AE signal parameters.

Each set of time signals from the two Minhorst sensors was checked visually to get the exact arrival time differences which are necessary for the source localization.

3 Experimental Results

3.1 AE during loading DCB specimens

Some DCB specimens were loaded up to about 80% of the fracture load and were then deloaded, whereas some other specimens were loaded up to macroscopic crack growth or rupture. The AE arose near to the maximum of the load. Although some of the specimens exhibited no crack after the loading, they had emitted about 3100 events (mean value for one specimen). The frequency distribution of the peak amplitudes is shown in Fig. 3(a). Both distributions for uncracked and cracked specimens are nearly parallel and can be approximated by a straight line in double-logarithmic scale. On the right side the distributions are cut due to saturation of the equipment. By performing fracture experiments with lower sensitivity on the bending specimens it can be seen that the amplitude distribution is unimodal (Fig. 3(b)). It contains no second maximum at higher amplitudes.

By small angle X-ray scattering (SAXS) measurements before and after the loading it has been shown that the number of scattering centres near to the notch increased clearly by loading[6] (Fig. 4). By turning the X-ray focus line, it has been found that these scattering centres had a preferred orientation parallel to the notch plane.

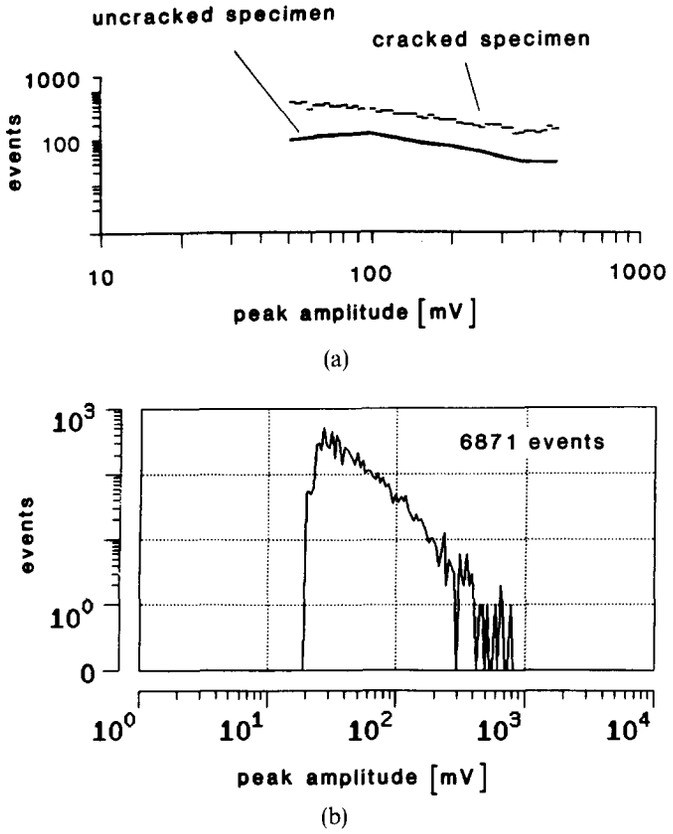

Fig. 3. Peak amplitude distributions of (a) DCB specimen and (b) SENB specimen.

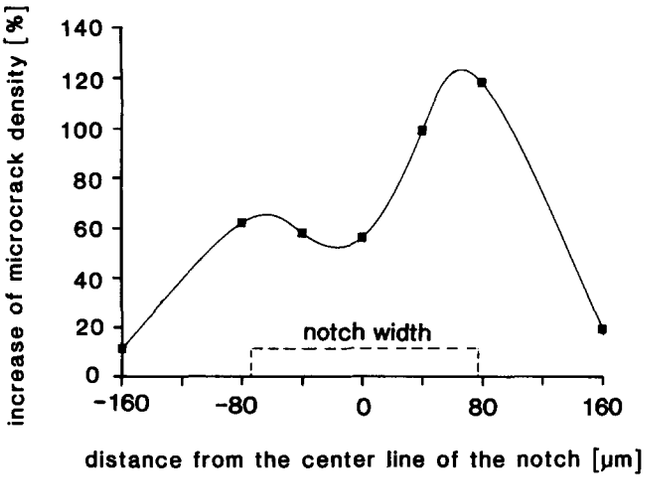

Fig. 4. Increase of microcrack density in the region of 300 μm around the notch root (after Ref. 6).

3.2 Risetime distributions

In some cases the shape of the frequency distribution of the AE signal parameters gives some information on the type of AE sources. In Fig. 5 the risetime distribution of cracked and uncracked DCB specimens can be compared. Both distributions exhibit two maxima. For the uncracked specimens the maximum at higher risetimes contains about 8% of all events, whereas the corresponding maximum for the cracked specimens contains 14%. Generally a

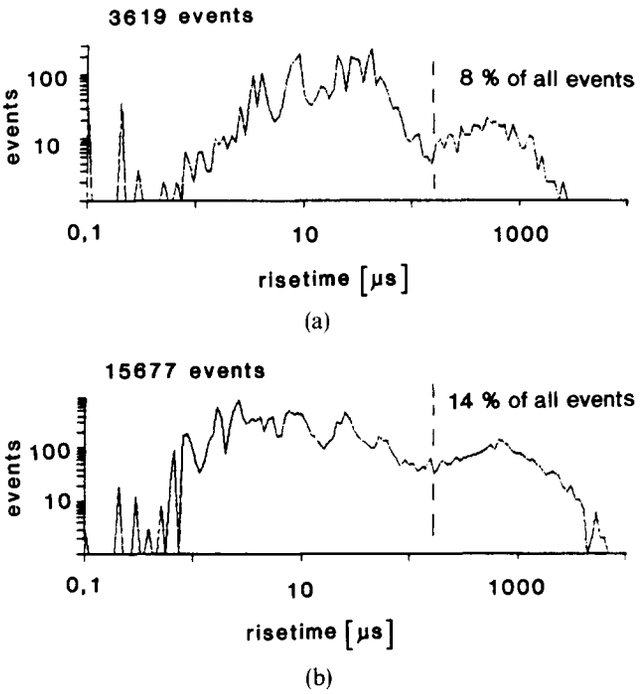

Fig. 5. Risetime distributions of (a) uncracked and (b) cracked DCB specimen.

bimodal distribution points to the fact that two different types of AE sources exist.

The origin of the two risetime maxima can be found by analysing the AE time signals. Most AE events consist of only one signal, but in some cases event clusters can be found. Figure 6 gives an example of a corresponding time signal. Within a time of 819 μs at least five individual events with small gaps between them are found. These five events are regarded as only one event by the hardware signal processor (see above) whose dead time was 819 μs. Whereas the mean event rate is 3–4 Hz at this experimental phase, the rate of the individual events in the displayed time window amounts to about 6000 Hz. Thus, it can be concluded that the individual events within one cluster are physically connected to one another. The probability of an accidental meeting of independent events within this short time window would be too low. The example in Fig. 6 shows that the individual event with the highest amplitude is the last. That means that the risetime of this event cluster as defined above is much larger than for an individual event.

Thus, it is clear that the first maximum at low risetimes in Fig. 5 is due to individual events whereas the second maximum is generated by event clusters. This has also been confirmed by direct comparison between time signals and the corresponding signal parameter data. Similar observations have also been made in thermal shock tests on a pressure vessel

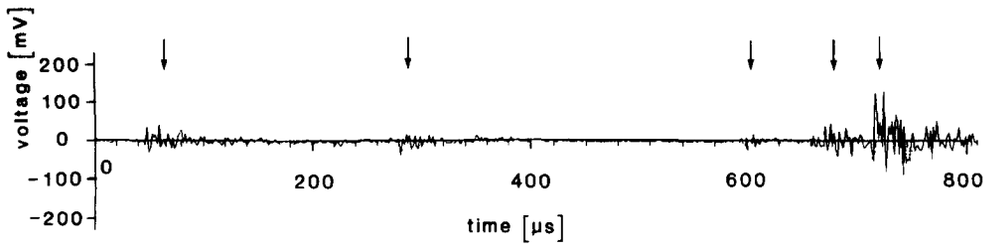

Fig. 6. Signal cluster (broadband transducer). ↓, Signal; crackdepth = 0·03 mm.

made from steel.[8] With regard to the risetime distribution it would appear that two source mechanisms of AE during crack propagation exist.

3.3 Source location and source types

Figure 7 shows the beginnings of time signals captured by the transducers 1 and 2 (Fig. 2). The very beginnings of the signals are clearly defined. The maximum of the first oscillation is reached within 200 ns. This corresponds to the time constant of the system configuration used here. This means that the lifetime of the AE sources amounts to ≤ 200 ns. For the determination of the time difference between the two signals, the mean value of the time differences of both the signal beginnings and the maxima of the first oscillations are used. Signals whose beginnings are not clearly defined are not taken into account.

Three different signal types have been found which differ with regard to their signal form and source position. The signals in Fig. 7 exhibit negative polarities on both sensors at the signal beginnings (type 1). Signal type 2 possesses a positive polarity on one sensor and a negative on the other. Type 3 has positive polarities on both sensors. In most cases the signal shapes of the three types are nearly the same except for the polarity.

Figure 8 displays the location distributions in the crack plane for different crack depth domains (sum of the crack propagation experiments of two specimens). On the top the positions of crack, notch and specimen edge at beginning of the crack growth are shown, whereas the scheme on the bottom describes the conditions at test end. In this representation the crack tip is positioned at 0 mm and

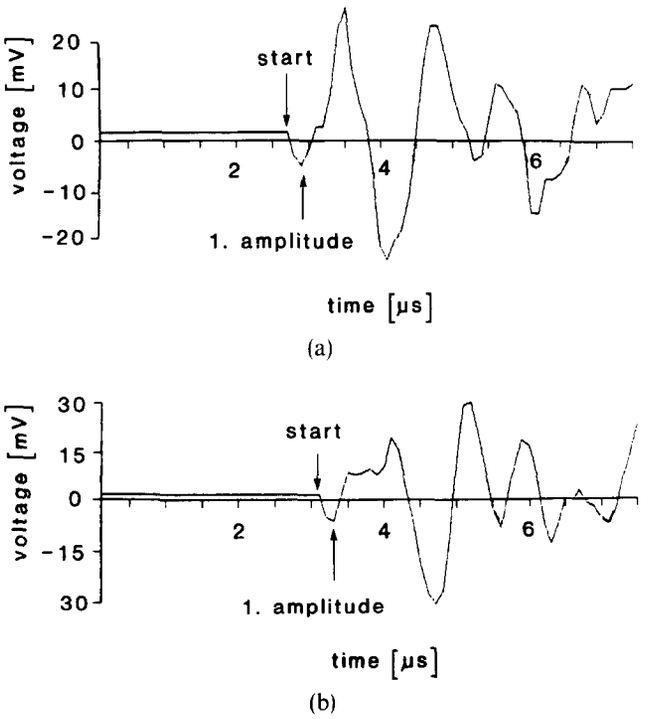

Fig. 7. Time signals of the transducers (a) 1 and (b) 2 with negative polarities at signal start. Crack depth = 5·2 mm.

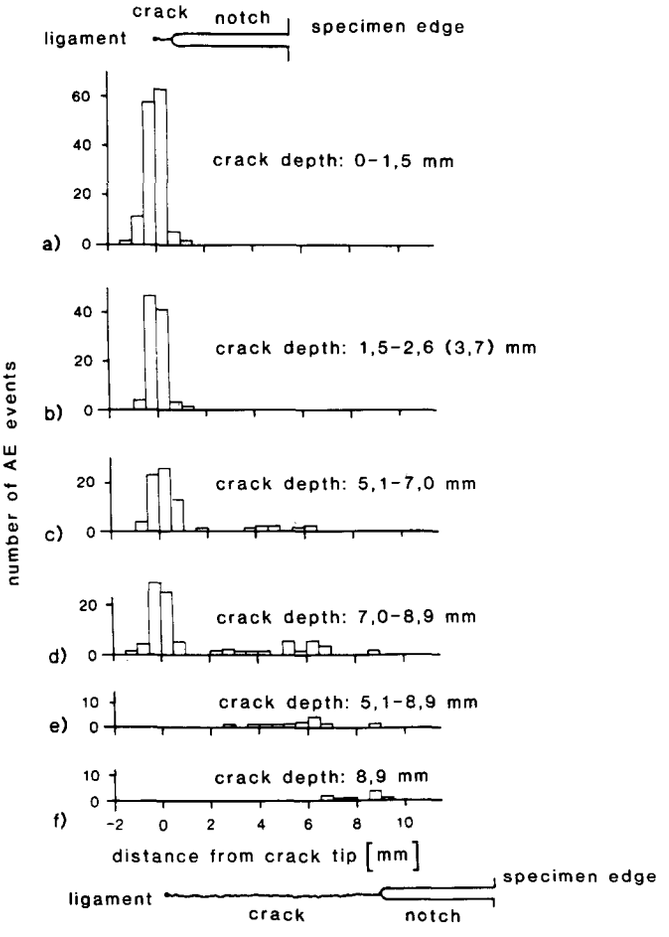

Fig. 8. Distributions of source locations referring to the crack tip. (a)–(d) All located events; (e) only events with opposite polarities on both transducers; (f) events at deloading (crack closure).

is fixed throughout the whole test. In Fig. 8(a)–(d), i.e. at crack depths of 0–9 mm, a location distribution can be observed at the crack tip with a half width of about 1 mm. As already mentioned, this is given by the inaccuracy of location and not by the process zone diameter of approximately 300 μm. This distribution represents the crack tip activity. Besides this, at crack depths of more than 5 mm a smooth distribution with a low number of events whose maximum is 5–6 mm away from the crack tip can be found. Thus, this distribution represents the AE activity at the crack flanks. On the right side of the crack tip, i.e. in the uncracked ligament, no events are found. Approximately 10% of all located events in the crack depth domain of 5·1–7·0 mm can be associated with the crack flanks (Fig. 8(c)). This percentage increases to about 20% in the domain of 7·0–8·9 mm (Fig. 8(d)). Similar proportions are also true for the AE energies.

An evaluation of the located events with respect to the signal polarities shows that the crack tip domain contains only signals of type 1, whereas both types 1 and 2 are detected in the crack flank domain. Figure 8(e) shows that type 2 is restricted to the crack flanks. Type 3 has been detected exclusively during deloading of a cracked specimen at the large crack depth of 8·9 mm (Fig. 8(f)). The maximum of the corresponding location distribution is found approximately 8 mm away from the crack tip.

4 Discussion of the Results

4.1 Formation of microcracks

The experiments in Section 3.1 show that there is an AE before the formation of a macrocrack but in combination with an increase of the number of scattering centres as found by the SAXS method. Since these centres have a preferred orientation parallel to the macroscopic crack plane and the main load axis is perpendicular to the crack plane, it can be concluded that the scattering centres are due to microcracks which have been generated during loading, since the orientation of the crack areas of the microcracks is expected to be preferably parallel to the notch area. The formation of the microcracks is accompanied by the observed AE.

4.2 Detection limits of the AE

According to crack propagation experiments on double torsion and bending specimens a minimum detectable crack velocity of 1–10 μm/s has been found. Kishi *et al.*[9] find the value of about 15 μm to be the minimum detectable crack size (crack diameter). The present authors' estimations, which take into account the measured crack size distribution, the size of the specimen volume damaged by the microcracks around the main crack and the proportion of microcracks as a function of the grain bevels,[3] yield a value of approximately 14 μm for the high sensitivity AE measurement on the DCB specimens and of $\geq 34\,\mu$m for the less sensitive measurement with the sensors 1 and 2 on the SENB specimens (Fig. 2). The grain size distribution of the material under investigation shows that the largest grains exhibit diameters of up to 100 μm. That means that for both sensitive and less sensitive measurements, the bevel fracture of the larger grains can be detected. The presupposition made here is that one bevel fracture generates one AE event.

4.3 Amplitude distribution

This presupposition appears to be approximately justified by analysing the distributions of grain sizes and peak amplitudes. Grain size distributions of the investigated material exhibit a log-normal behaviour. The right and left flank of this distribution can be approximated by a straight line in a double-logarithmic scale.[10] The right flank of the AE peak amplitude distribution can also be approximated by a straight line ((Fig. 3(b)). The left flank is given by the detection threshold. Thus, it can be concluded that the observed peak amplitude distribution is the extreme right part of an log-normal distribution whose major part on the left is not detectable. Crack area F and peak amplitude a_m are related by

$$a_m \propto F^x$$

with $x \sim 1$–$1{\cdot}5$.[11] The similarity of the distributions of grain size and amplitudes points to the fact that the crack mode of the investigated material is determined by the fracture of grain bevels whose size is closely connected to the grain size.

4.4 Coalescence of microcracks

As already shown the amplitude distribution is unimodal, whereas the risetime distribution is bimodal. It can be presumed that the individual events represent the formation of unconnected microcracks, whereas the event clusters are due to the coalescence of microcracks. From AE characteristics it can be concluded that such a coalescence event does not occur in one big single step but in a series of smaller microcrack formation events with small time intervals between the individual microcracks events. The amplitudes of the events within an event cluster are similar to the amplitudes of the

individual events. Therefore single microcrack events and coalescence events can be distinguished by analysing the risetime distribution but not by amplitude distribution.

During the initial formation of the process zone mainly individual microcracks are to be expected. With increasing size of the process zone more and more coalescence events should occur. This is actually observed by the increasing second maximum of the risetime distribution with load (Fig. 5).

4.5 Radiation pattern of AE sources

The different polarities of the signal beginnings can be explained by the radiation pattern of AE events during cleavage and shear cracking.[12] Cleavage cracking (mode I) exhibits the same polarity of sound pressure in all directions (Fig. 9(a)) whereas the largest sound amplitude is found perpendicular to the cleavage source. By test signals it has been verified that a compressive wave generates a negative signal start at the experimental set-up used here. Microcracking also generates compressive waves by an increase of crack volume. Thus the signals of type 1 can be assigned to microcracking. Signal type 3, with its positive signal starts, has been observed only at specimen deloading where no crack growth is to be expected. The reverse polarity compared to type 1 points to an abrupt local decrease of crack volume. Presumably at deloading the approaching crack surfaces are hindered by protruding grains or debris from closing completely (crack closure effect). Continuing the deloading, these spots are crushed abruptly. This event produces a quick volume decrease and thus an AE signal of type 3.

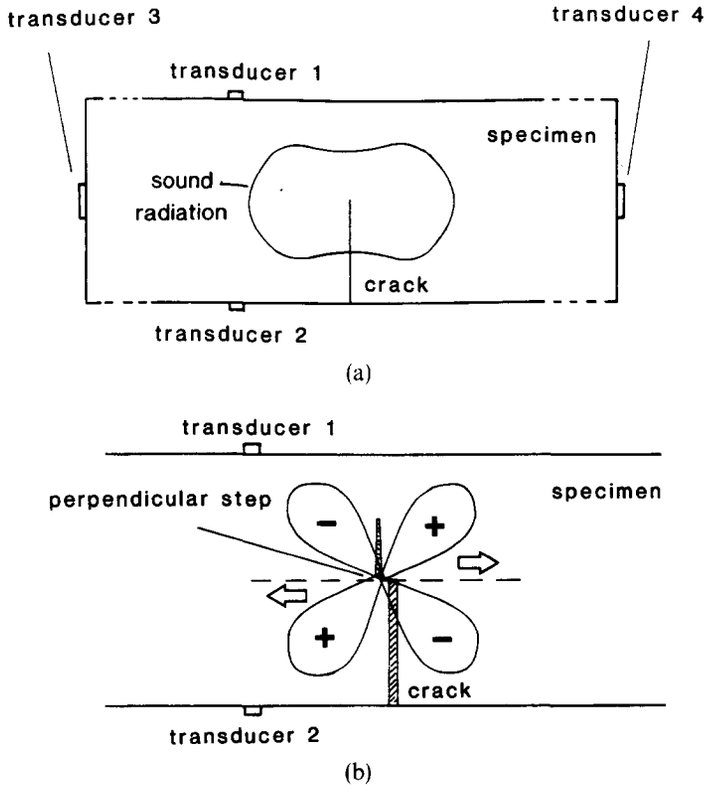

Fig. 9. Radiation pattern of AE sources for longitudinal waves: (a) Microcrack source and (b) shear source.

Figure 9(b) shows the radiation pattern for a shear source (mode II or III). Here a slip off on a step standing perpendicular to the macroscopic crack face is assumed. Four sound lobes with alternating polarities are found. The transducers 1 and 2 are arranged in such a manner that they capture the sound radiation of two different polarized sound lobes. An AE event with different polarities of the signal beginnings (type 2) results from such a shear event. The two AE signal types found in the wake of the crack tip can thus be interpreted by slip and friction events (signal type 2) at interacting points of the crack surface and by secondary crack formation around these interacting points (type 1). Some indications for slip events in the crack flank domain in alumina have also been found by optical[13] and acoustical[14] microscopy.

The region adjacent to the crack surface is subjected to compressive stresses which are generated by the volume dilatation due to the microcracks.[2] If some of the energy stored in this region is released quickly by a shear crack it would produce an AE event with the radiation pattern of signal type II on one side of the specimen. However, on the other side the sound waves would be reflected at the surface of the main crack, and they would not arrive at the sensors on the other specimen side (Fig. 2). Thus, only one of the sensors near to the crack would be hit, and no locateable AE event results. Hence, the signals from type II are obviously generated by events located in the crack surface and not inside the seam around it.

4.6 Location distribution in the crack flank domain

According to Fig. 8 a smooth location distribution is found inside the crack flank domain for crack depths beyond 5 mm. The maximum of this distribution lies 5–6 mm away from the crack tip. At small crack depths no crack flank events are observed, but the decisive crack resistance increase in alumina arises at a crack depth which is distinctly smaller than 5 mm.[1] Therefore, it could be concluded that the crack flank events found by AE are not essential for the crack resistance increase.

However, this conclusion is not convincing if one takes into account that usually only one part—very often the minor part—of the total AE is detectable.

For instance, this can be seen for the distribution of peak amplitudes which reflects the distribution of microcrack sizes (see 4.3, Fig. 3) at the crack tip: only the extreme right part of the amplitude distribution is detectable. It can be presumed that this is also true for the distribution of crack flank events.

For simplicity it is assumed here that there are two major types of interaction sites at the crack flanks which are shown schematically in Fig. 10. The first type represents small interaction sites whose loosening—by breakage or friction—releases small energies and therefore generates small AE amplitudes and thus cannot be detected by AE testing (Fig. 10(b)). The large interaction sites, however, generate a detectable AE at loosening. To loosen these interaction sites, a large crack opening is necessary which is to be found at large distances between the crack tip and interaction sites (d_2 in Fig. 10(a)). On the other hand, the small interaction sites loosen near to the crack tip (distance d_1 in Fig. 10(a)). That is the reason why the observed crack flank events are only found far away from the crack tip (observed distribution in Fig. 10(c)). They represent only the minority of crack flank events. The majority arises near to the crack tip but is not detectable (idealized distribution in Fig. 10(c)).

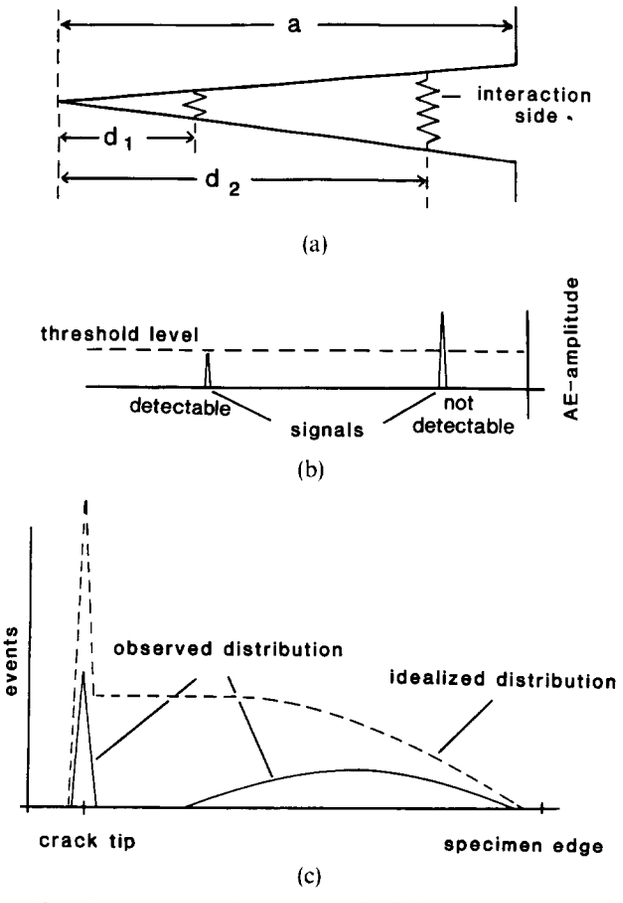

Fig. 10. Schematic illustration of AE from crack flanks.

At present it is not possible to estimate the proportion of undetectable crack flank events, but the general conclusion can be drawn that these events contribute to the increase of crack resistance.

5 Conclusions

From AE results is can be concluded that a process zone formed around the notch tip and consisting of microcracks is generated with increasing load. This zone may determine the starting value of the crack resistance. With increasing load the microcracks coalesce and produce the macrocrack. This is done not by a large single step but by several smaller steps. At a crack depth of about 5 mm some energy dissipation in the crack flanks is observed which indicates that the crack flanks contribute to the increase of crack resistance. It can be assumed that this energy dissipation exists at smaller crack depths, too. However, it cannot be detected by AE due to unsufficient sensitivity since energy dissipation is too low. Thus from the viewpoint of AE both the process zone at the crack tip and interactions at the crack flanks determine the crack resistance, but the relative contributions of both mechanisms cannot yet be given.

Acknowledgements

This work was supported by the Deutsche Forschungsgemeinschaft (DFG). The author wishes to acknowledge the contributions made by many colleagues from Forschungszentrum Jülich, Institut für Werkstoffmechanik Freiburg, Universität Dortmund, Technische Hochschule Darmstadt and Institut für zerstörungsfreie Prüfverfahren Saarbrücken.

References

1. Bär, K. K. O., Kleist, G. & Nickel, H., Mikrobruchvorgänge in Al_2O_3-Keramik, DFG-Abschlußkolloquium, Jülich, FRG, Apr. 9–10, 1990, Konferenzen des Forschungszentrums Jülich, Ed.: Forschungszentrum Jülich GmbH, Vol. 7, 1991, 197–220.
2. Buresch, F. E., Fortschrittsberichte der Deutschen Keramischen Gesellschaft, Ceramic Forum International, Bad Honnef, FRG, Vol. 5, 1990, Heft 1, 241–253.
3. Buresch, F. E., *Materialprüfung*, **29** (1987) 261–8.
4. Deuerler, F., Knehans, R. & Steinbrech, R., *Science of Ceramics*, **13** (1985).
5. Knehans, R. & Steinbrech, R., *Fortschrittsberichte der Deutschen Keramischen Gesellschaft*. Ceramic Forum International, 1985, pp. 59–70.
6. Babilon, E., Kleist, G. & Nickel, H., see (1), 175–196.

7. Hepp, K. & Waschkies, E., FhG-Berichte 3/4-85, Fraunhofer-Edition, München, FRG, ed. W. Zitzelsberger, 1985, 36–41.
8. Sklarczyk, C. & Waschkies, E., *Journal of Acoustic Emission*, **8** (1989) S93–S96.
9. Kishi, T., Wakayama, S. & Kohara, S., *Fracture Mechanics of Ceramics*, **8** (1986) 85–100.
10. Erlenkämper, S., *Acoustic Emission*. Deutsche Gesellschaft für Metallkunde, Oberursel, FRG, 1980, pp. 165–88.
11. Evans, A. G., Fundamentals of Acoustic Emission, In *Proc. of a Joint Meeting of the Acoustic Societies of America and Japan*, Honolulu, Hawaii, 27 November–1 December 1978, ed. K. Ono, pp. 209–27. UCLA School of Eng. and Appl. Sci., 1979,
12. Savage, J. C., *Bulletin of the Seismological Society of America*, **55** (1965) 263–75.
13. Swanson, P. L., Fairbanks, C. L., Lawn, B. R., Mai, Y.-W. & Hockey, B. J., *J. Amer. Ceram. Soc.*, **70** (1987) 279–89.
14. Quinten, A. & Arnold, W., *Mat. Sci. Eng.*, **A122** (1989) 15–19.